Model of reversible vesicular transport with exclusion

Paul C Bressloff and Bhargav R Karamched

Department of Mathematics, University of Utah 155 South 1400 East, Salt Lake City, UT 84112, USA

E-mail: bressloff@math.utah.edu and karamche@math.utah.edu

Abstract

A major question in neurobiology concerns the mechanics behind the motor-driven transport and delivery of vesicles to synaptic targets along the axon of a neuron. Experimental evidence suggests that the distribution of vesicles along the axon is relatively uniform and that vesicular delivery to synapses is reversible. A recent modeling study has made explicit the crucial role that reversibility in vesicular delivery to synapses plays in achieving uniformity in vesicle distribution, so called synaptic democracy (Bressloff *et al* 2015 *Phys. Rev. Lett.* **114** 168101). In this paper we generalize the previous model by accounting for exclusion effects (hard-core repulsion) that may occur between molecular motor-cargo complexes (particles) moving along the same microtubule track. The resulting model takes the form of an exclusion process with four internal states, which distinguish between motile and stationary particles, and whether or not a particle is carrying vesicles. By applying a mean field approximation and an adiabatic approximation we reduce the system of ODEs describing the evolution of occupation numbers of the sites on a 1D lattice to a system of hydrodynamic equations in the continuum limit. We find that reversibility in vesicular delivery allows for synaptic democracy even in the presence of exclusion effects, although exclusion does exacerbate nonuniform distributions of vesicles in an axon when compared with a model without exclusion. We also uncover the relationship between our model and other models of exclusion processes with internal states.

Keywords: axonal transport, synaptic democracy, exclusion processes, mean field approximation, TASEP

(Some figures may appear in colour only in the online journal)

1. Introduction

A fundamental question in cell biology concerns the mechanism behind the delivery of newly synthesized macromolecules to specific regions of the cell membrane [2]. Such processes are necessary, for example, when the cell requires proteins for ion channel construction or when, in the case of neurons, materials are needed for synaptogenesis. Indeed, the problem of the transportation of macromolecules to cell membranes is particularly acute in neurons due to the wide variety of sizes that are exhibited by them—in humans they can range from a micron to a meter in length. Moreover, neurons can have a highly complex branched structure that renders vesicular delivery to localized regions of the cell membrane even more difficult.

Axons and dendrites both contain protein-rich synaptic subcellular compartments that form synaptic contacts between neurons. Some of the synaptic junctions occur along the body of the axon—*en passant* synapses—while others occur at the terminals of axonal branches. Generation of new synaptic contacts during synaptogenesis or modification of old synapses in response to synaptic activity require localized protein delivery to a particular synaptic site [3, 16]. The relatively long distance between the soma and the distal axonal or dendritic synapses necessitates the use of active transport as the means for vesicular delivery; passive processes such as diffusion would take too long. Active transport in the intracellular space generally involves microtubules—the highways of the cell—and molecular motors—the delivery vehicles. Microtubules are directionally polarized filaments with biophysically distinguishable (+) ends and (−) ends. The type of polarity at a given end of the microtubule dictates what kind of molecular motor will travel along the microtubule in a given direction. For example, kinesin motors generally carry their cargo along microtubules in the (+) direction whereas dynein motors tend to move towards the (−) end [15]. Delivery of several components across the neuron is accomplished by means of this active transport machinery [13], and breakdown of active transport has been implicated in many neurodegenerative diseases such as Alzheimer's and Parkinson's [8].

One issue we seek to investigate here concerns the neuron's ability to evenly distribute vesicles across its *en passant* synapses. Considering the fact that the source of the motors that deliver these cargo to the synapses is the soma of the neuron, one would expect that synapses located proximally to the soma would obtain a greater amount of cargo compared to the distal axonal or dendritic synapses. One way a more democratic distribution of resources could be achieved is by tagging cargo with molecular addresses that route molecular motors to the required synapse, but there is no known mechanism that functions in this manner. Recent experimental studies of axons in *C. elegans* and *Drosophila* have shown the following: (i) motor-driven cargo exhibits ballistic anterograde or retrograde motion interspersed with periods of long pauses at presynaptic sites; (ii) the capture of vesicles by synapses during the pauses is reversible, in that vesicular aggregation at a site could be inhibited by signaling molecules resulting in dissociation from the target [20, 26]. In a recent paper, this phenomenon was studied mathematically in terms of an advection–diffusion model of vesicular transport [3]. Given a source of vesicle-bound, motor-cargo complexes (particles) at one end of an axon, the steady-state distribution of synaptic vesicles along the axon was found to be a decaying exponential when vesicular delivery to synapses was irreversible, whereas an approximately uniform distribution was obtained in the case of the reversible exchange of vesicles between particles and synaptic targets. However, one potential limitation of the previous advection–diffusion model is that it does not account for any hard-core interactions between particles traveling along the same microtubule track.

In this paper, we generalize the results of [3] by considering the effects of exclusion between particles on the steady-state distribution of synaptic vesicles. As in [3], we compare

the effects of reversible and irreversible vesicular delivery on this distribution. We treat the axon as a one-dimensional lattice and model the motion of vesicle-bound particles with ordinary differential equations (ODEs) for the expected occupation number at each lattice site. We also assume that each lattice site has a corresponding synapse to which the particle occupying the site can deliver its cargo. In the irreversible case, we use a mean field approximation to recast the original model as a nonlinear partial differential equation (PDE) reminiscent of the hydrodynamic equations that appear in models of totally asymmetric exclusion processes (TASEP). We find that exclusion effects exacerbate the preferential delivery to proximal synapses when compared to the results of no exclusion obtained in [3]. For the reversible delivery case, we allow particles to randomly switch between a motile and stationary state. In contrast to the irreversible case, we also keep track of the motion of particles that are not carrying any vesicles. Hence, the resulting exclusion process has four internal states. The mean field approximation again allows for TASEP-like hydrodynamic equations which, under an adiabatic approximation, can be solved exactly. We find that reversibility in cargo delivery allows for a more homogeneous distribution of vesicles, provided that the presence of a vesicle bound to a motor-cargo complex does not significantly change its speed (hopping rate).

The structure of the paper is as follows. We first briefly recount the analysis and results found in [3] (section 2). In section 3 we introduce our single-state model of irreversible vesicular transport with exclusion, and show how it maps on to a TASEP. We then turn to the four-state model of reversible vesicular transport with exclusion (section 4). Finally, in section 5 we briefly relate our model to other models that investigate driven exclusion processes, where internal states are assigned to particles occupying each lattice site, for example [27, 28]. However, it should be noted that in contrast to these other studies, the emphasis of our paper is not to construct phase diagrams as a function of model parameters such as the inward and outward fluxes. Rather, we are interested in the particular question of how exclusion effects alter the steady-state distribution of synaptic vesicles.

2. Vesicular transport without exclusion

Before elucidating our model and results, we briefly present the results found in [3].

2.1. Irreversible delivery

Consider a population of motor-cargo complexes or particles moving on a semi-infinite track, each of which carries a single synaptic vesicle precursor (SVP) to be delivered to a synaptic site. Assume that these particles are injected at the soma ($x = 0$) at a fixed rate J_1 and that the distribution of synaptic sites along the axon is uniform. That is, at any given spatial point x, a particle can deliver its cargo to a synpase at a rate k. Neglecting interactions between particles, the dynamics of the motor-cargo complexes can be captured by the advection–diffusion equation [3]

$$\frac{\partial u}{\partial t} = -v\frac{\partial u}{\partial x} + D\frac{\partial^2 u}{\partial x^2} - ku, \qquad x \in (0, \infty), \tag{2.1}$$

where $u(x, t)$ is the particle density along the microtubule track at position x at time t. Note that equation (2.1) can be derived from more detailed biophysical models of motor transport under the assumption that the rates at which motor-cargo complexes switch between different motile states are relatively fast [3, 23]. In particular, the mean speed will depend on the relative times that the complex spends in different anterograde, stationary, and possibly

retrograde states, whereas the diffusivity D reflects the underlying stochasticity of the motion. Equation (2.1) is supplemented by the boundary condition at $x = 0$:

$$J(u(0, t)) = J_1, \quad J(u) \equiv vu - D\frac{\partial u}{\partial x}. \tag{2.2}$$

Let $c(x, t)$ denote the concentration of delivered vesicles to the presynaptic sites at x at time t with

$$\frac{\partial c}{\partial t} = ku - \gamma_c c, \tag{2.3}$$

where γ_c denotes the degradation rate for vesicles. Note that in the irreversible delivery case, including vesicular degradation is necessary to prevent blowup in the solutions for $c(x, t)$. This consideration is not necessary in the reversible delivery case. The steady state solution for c is given by

$$c = \frac{k}{\gamma_c} \frac{J_1 e^{-x/\xi}}{D/\xi + v} \qquad \xi = \frac{2D}{-v + \sqrt{v^2 + 4Dk}}, \tag{2.4}$$

which clearly indicates that c decays exponentially with respect to distance from the soma with correlation length ξ. For values of D and v that are relevant to cytoplasmic transport, we see that $\xi = O(1/k)$, meaning that k must be on the order of $10^{-4}\,\mathrm{s}^{-1}$ to make ξ comparable to typical axonal lengths. Measured values of k, however, tend to be on the order of a few inverse minutes [3, 14, 18]. This result is inconsistent with the experimental evidence found regarding uniform vesicular distribution in the axons of *C. elegans* and *Drosophila* [20, 26]. We now show, following [3], that relaxing the irreversible delivery condition in this model allows for a more uniform distribution of vesicles along the axon.

2.2. Reversible delivery

In order to take into account the reversibility of vesicular delivery to synapses, one must consider a generalization of the advection–diffusion model (2.1). To that end, let $u_0(x, t)$ and $u_1(x, t)$ denote the density of motor-cargo complexes without and with an attached SVP, respectively, and let k_+ and k_- denote the rates at which vesicles are delivered to synaptic sites and recovered by the motors, respectively. Each density evolves according to an advection–diffusion equation combined with transition rates that represent the delivery and recovery of SVPs:

$$\frac{\partial u_0}{\partial t} = -v_0 \frac{\partial u_0}{\partial x} + D\frac{\partial^2 u_0}{\partial x^2} - \gamma_0 u_0 + k_+ u_1 - k_- c u_0, \tag{2.5a}$$

$$\frac{\partial u_1}{\partial t} = -v_1 \frac{\partial u_1}{\partial x} + D\frac{\partial^2 u_1}{\partial x^2} - \gamma_1 u_1 - k_+ u_1 + k_- c u_0, \tag{2.5b}$$

with $x \in (0, \infty)$. Disparity in the velocities in each state reflects the effect cargo can have on particle motility, while the degradation rates $\gamma_{0,1}$ are included to account for the possibility of particle degradation or recycling. Equations (2.5a) and (2.5b) are supplemented by the boundary conditions

$$J(u_j(0, t)) = J_j, \qquad j = 0, 1, \tag{2.6}$$

where J_j is the constant rate at which particles with or without cargo are injected into the axon from the soma. The dynamics for $c(x, t)$ are now given by
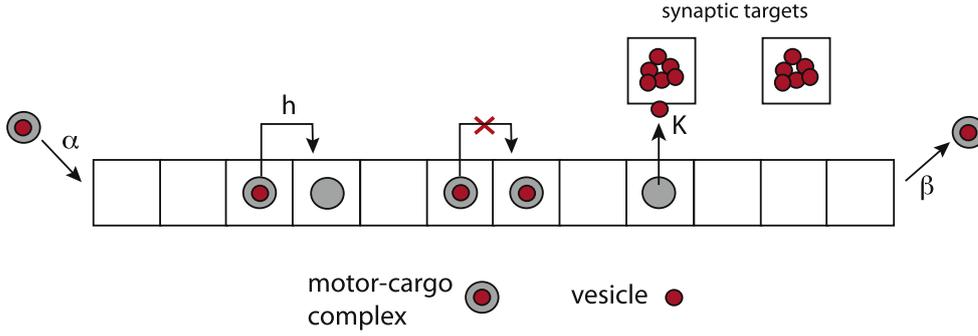
Figure 1. Dynamical rules for irreversible vesicular transport: hopping, irreversible exchange of vesicles with synaptic targets, and entry/exit rates.

$$\frac{\partial c}{\partial t} = k_+ u_1 - k_- c u_0. \tag{2.7}$$

We need not explicitly include degradation in this case because, provided $J_0 > 0$, $c(x, t)$ will be bounded. The steady state distribution of vesicles is then

$$c = \frac{k_+ u_1}{k_- u_0}.$$

Substitution into the steady state analogs of equations (2.5a) and (2.5b) yields

$$u_j(x) = \frac{J_j e^{-x/\xi_j}}{D/\xi_j + v_j} \qquad \xi_j = \frac{2D}{-v_j + \sqrt{v_j^2 + 4D\gamma_j}} \tag{2.8}$$

whence

$$c = \frac{k_+}{k_-} \frac{J_1}{J_0} \frac{D/\xi_0 + v_0}{D/\xi_1 + v_1} e^{-\Gamma x}$$

with $\Gamma \equiv \xi_1^{-1} - \xi_0^{-1}$. It is evident that if $\Gamma = 0$, then c has a spatially uniform distribution.

In summary, introducing reversibility in vesicular delivery provides a means for a more uniform distribution amongst the *en passant* synapses [3]. However, there are certain limitations of this minimal model: (i) the exclusion effects of motor-cargo complexes that have delivered a synaptic vesicle are ignored; (ii) the fact that particles switch between different motile states is ignored, in particular, vesicular exchange with synaptic targets is only likely to occur when a particle is stationary. Before presenting the full four-state model of reversible cargo delivery that combines both of these features (see section 4), we first investigate the effects of exclusion on a simpler single-state model with irreversible cargo delivery.

3. Irreversible vesicular transport with exclusion

Consider a motor-cargo complex hopping unidirectionally along a one-dimensional track, see figure 1. We represent the track as a lattice of N sites, labeled $i = 1, \ldots, N$, with lattice spacing $\varepsilon = L/N$, where L is the length of the track. For simplicity, we assume that each particle can only carry a single cluster of vesicles, and that we ignore partial delivery of a cluster, that is, it is 'all-or-none.' In the following, we represent a vesicular cluster by a single vesicle. Each site is either vacant or occupied by a vesicle-bound particle, and the particle can hop to the right if

and only if the adjacent site is vacant (hard exclusion). At each site a particle can irreversibly deliver its vesicle(s) to a synaptic target at a rate K and the corresponding site becomes vacant. In other words, we assume that a motor-cargo complex without vesicles does not obstruct the movement of other particles. (This simplification will be removed in our full model, see section 4.) We specify the state of the site i in terms of the occupation number $n_i \in \{0, 1\}$ with $n_i = 1$ if the ith site is occupied by a vesicle-bound motor-cargo complex and zero otherwise. The hopping rate of a particle is taken to be h. We assume that particles are injected on the left-hand boundary at a rate α, and exit the right-hand boundary at a rate β with $0 < \alpha, \beta < h$. Finally, we assume that each lattice site $i \neq 1, N$ has an associated synaptic target with c_i vesicles (taken to be large so that c_i is treated as a continuous variable).

Within the context of intracellular motor transport, one typically interprets the particle as a single molecular motor and the track as a single microtubular filament, with the fundamental length-scale (lattice spacing) given by a single step of a motor, which is around 10 nm [5]. Here, however, we are interested in the transport of motor-cargo complexes along axons, and the delivery of vesicular cargo to synaptic targets. This means that we are looking at processes occurring on significantly longer length-scales. First, we take a single particle to be a macromolecular complex consisting of multiple motors bound to a cargo. Such a complex could have a size of around $0.1 - 1\ \mu$m, which is comparable to the size of a synaptic target. Therefore, for concreteness, we take the lattice spacing to be $\varepsilon = 1\ \mu$m. Second, the 1D track is now identified with an axon of length L that could extend for several mm. (For simplicity, we assume that the transfer of motors from one MT to the next along an axon is smooth.) It is important to note that one major simplification of our discrete hopping model is that we are replacing a single continuous run of the motor-cargo complex by a single hop over a distance of ε. We are also assuming that the particle stops at regularly spaced synaptic sites. A more complex, hetereogeneous model would distinguish between the size of the complex, the spacing of synaptic targets, and the fundamental lattice spacing.

We are interested in determining macroscopic properties of the above exclusion process, in particular, the steady-state density profiles (average occupancies of each lattice site) and the distribution of synaptic vesicles. The density of motor-cargo complexes is denoted by $\langle n_i \rangle$. Here the angular brackets denote the average with respect to all histories of the stochastic dynamics, which can be interpreted as an ensemble average over a large set of trials starting from the same initial conditions. Away from the boundaries, the dynamics is described by the following system of equations for $1 < i < N$:

$$\frac{d\langle n_i \rangle}{dt} = \langle n_{i-1}(1 - n_i) \rangle - \langle n_i(1 - n_{i+1}) \rangle - K\langle n_i \rangle. \tag{3.1}$$

At the boundaries we have

$$\frac{d\langle n_1 \rangle}{dt} = -\langle n_1(1 - n_2) \rangle + \alpha\langle 1 - n_1 \rangle, \tag{3.2a}$$

$$\frac{d\langle n_N \rangle}{dt} = \langle n_{N-1}(1 - n_N) \rangle - \beta\langle n_N \rangle. \tag{3.2b}$$

Note that we have fixed the unit of time so that the hopping rate $h = 1$. The number of vesicles at the ith synaptic target is taken to evolve according to the simple first-order kinetic scheme

$$\frac{dc_i}{dt} = K\langle n_i \rangle - \gamma c_i, \tag{3.3}$$

where γ is a vesicular degradation rate. (As highlighted in section 2, if we were to neglect degradation of synaptic vesicles, then we would have to impose a maximum capacity of synaptic targets, otherwise c_i could become unbounded. This is not an issue for reversible vesicular transport.) Note that if $K = 0$ (no delivery of vesicles to synaptic targets), then equation (3.1) reduces to the standard TASEP [1, 9–11, 17]. On the other hand, if $K > 0$, then it is equivalent to a limiting case of TASEP with langmuir kinetics [12, 24, 25], in which the motor binding rate is zero.

We will analyze the above model by using the hydrodynamic approach of Parmeggiani *et al* [12, 25]. As is well known, equation (3.1) constitutes a nontrivial many-body problem, since in order to calculate the time evolution of $\langle n_i \rangle$ it is necessary to know the two-point correlations $\langle n_{i-1} n_i \rangle$. The latter obey dynamical equations involving three-point and four-point correlations. Thus, there is an infinite hierarchy of equations of motion. However, progress can be made by using a mean-field approximation and a continuum limit in order to derive a PDE for the densities. The mean-field approximation consists of replacing two-point correlations by products of single-site averages:

$$\langle n_i n_j \rangle = \langle n_i \rangle \langle n_j \rangle.$$

Next we set $x = k\varepsilon$ and $\rho(x, t) = \langle n_k(t) \rangle$. The continuum limit is then defined according to $N \to \infty$ and $\varepsilon \to 0$ such that the length of the track $L = N\varepsilon$ is fixed. (We fix length scales by setting $L = 1$). Taylor expanding $\rho(x \pm \varepsilon, t)$ in powers of ε,

$$\rho(x \pm \varepsilon, t) = \rho(x) \pm \varepsilon \partial_x \rho(x, t) + \frac{1}{2}\varepsilon^2 \partial_{xx}\rho(x, t) + O(\varepsilon^3)$$

then gives to leading order in ε the following nonlinear PDE:

$$\frac{\partial \rho}{\partial t} = -\varepsilon \frac{\partial J(x, t)}{\partial x} - K\rho(x, t), \tag{3.4}$$

where

$$J(x, t) = \rho(x, t)(1 - \rho(x, t)) - \frac{\varepsilon}{2}\frac{\partial \rho(x, t)}{\partial x}, \tag{3.5}$$

and the boundary conditions are

$$J(0, t) = \alpha(1 - \rho(0, t)), \quad J(1, t) = \beta\rho(1, t).$$

Finally, the continuum limit of equation (3.3) is

$$\frac{\partial c(x, t)}{\partial t} = K\rho(x, t) - \gamma c(x, t). \tag{3.6}$$

3.1. Steady-state analysis

We wish to calculate the steady-state distribution of synaptic vesicles, which is given by

$$c(x) = \frac{K\rho(x)}{\gamma}, \tag{3.7}$$

with $\rho(x)$ the solution of the steady-state equation

$$(1 - 2\rho)\partial_x \rho - \frac{\varepsilon}{2}\partial_{xx}\rho = -\frac{K\rho}{\varepsilon}. \tag{3.8}$$

Following Parmeggiani *et al* [25], we drop the $O(\varepsilon)$ diffusion term and write the first-order ODE in the form

$$\partial_x[2\rho(x) - \ln \rho(x)] = \frac{K}{\varepsilon}. \tag{3.9}$$

The resulting boundary value problem is overdetermined as one still has to satisfy the boundary conditions at $x = 0, 1$:

$$\rho(0) = \alpha, \quad \rho(1)(1 - \rho(1)) = \beta\rho(1). \tag{3.10}$$

Note that the second boundary condition is satisfied if $\rho(1) = 1 - \beta$ or $\rho(1) = 0$. The standard procedure is to separately solve the ODE in the two domains $[0, x)$ and $(x, 1]$, imposing the left and right boundary conditions, respectively. The two solutions are matched in an $O(\varepsilon)$ neighborhood of some point x_0 using a boundary layer. (Within the boundary layer the density changes rapidly and one can no longer ignore the diffusion term.) This matching also determines the location of x_0. In our particular system, the physically relevant solutions decay (faster than) exponentially from the left-hand boundary $x = 0$ with some correlation length ξ (see below). Since $\xi \ll L$, it follows that we can effectively treat the domain as semi-infinite with $\rho(x) \to 0$ as $x \to \infty$. In particular, the solution is independent of β.

Integrating equation (3.9) in the two domains yields the left-end (*l*) and right-end (*r*) solutions

$$\rho(x)e^{-2\rho(x)} = Y_{l,r}(x), \tag{3.11}$$

with

$$Y_l(x) = \rho(0)e^{-Kx/\varepsilon - 2\rho(0)}, \quad Y_r(x) = \rho(1)e^{-K(x-1)/\varepsilon - 2\rho(1)}. \tag{3.12}$$

As noted in [25], equation (3.11) has an explicit solution expressed in terms of the so-called Lambert W function, $2\rho(x) = -W(-Y(x))$ with $Y(x) = 2Y_{l,r}(x)$. The Lambert W function [7] is a multi-valued function with two real branches as shown in figure 2. Since $\rho(x) \in [0, 1]$, it follows that

$$\rho(x) = \begin{cases} -\frac{1}{2}W_0(-Y(x)) & \rho \in [0, 0.5], \\ -\frac{1}{2}W_{-1}(-Y(x)) & \rho \in [0.5, 1]. \end{cases} \tag{3.13}$$

In contrast to [25], we do not assume that the degradation rate K is $O(\varepsilon)$ since this would yield unrealistically slow delivery rates (see below). This means that the left end function $Y_l(x)$ decays over a length-scale ξ (in physical units) such that $\xi \sim hL/(KN)$. If we take the effective length of the axon to be 10mm, the lattice spacing to be 1μ m, and the hopping rate to be $0.1 - 1$ s^{-1} (based on speeds of motor-cargo complexes [15]), then $\xi \sim K^{-1}$ μm with K measured in s^{-1}. Thus, in order to have correlation lengths comparable to axonal lengths of several millimeters, we would require delivery rates of the order $K \sim 10^{-4} - 10^{-5}$ s^{-1}, whereas measured rates tend to be of the order of a few inverse minutes [18, 19]. Therefore, in contrast to [25], $\xi \ll L$. Hence $Y_l(x) \approx 0$ when $\xi \ll x < L$. Similarly, the right end function $Y_r(x)$ grows exponentially over a distance ξ from $x = 1$. It is clear that the only physically relevant solution when $\alpha < 1/2$ is $\rho(x) = -W_0(-2Y_l(x))/2$ with $\rho(0) = \alpha$ and $\rho(1) = 0$. (Since $W_0(-Y)$ is a monotonically decreasing function of $|Y|$ with $W_0(-Y) \to 0$ as $Y \to 0$, it follows that the density $\rho(x)$ also decays over the length-scale within the bulk of the domain.) If $\alpha > 1/2$ then the left end solution $\rho(x) = -W_1(-2Y_l(x))/2$ cannot match the right-hand boundary condition, since $W_{-1}(-2Y_l) \to \infty$ as $Y_l \to 0$. Hence, there exists a boundary layer on the left-hand side that matches $\rho(0) = \alpha > 1/2$ with a bulk solution of the form
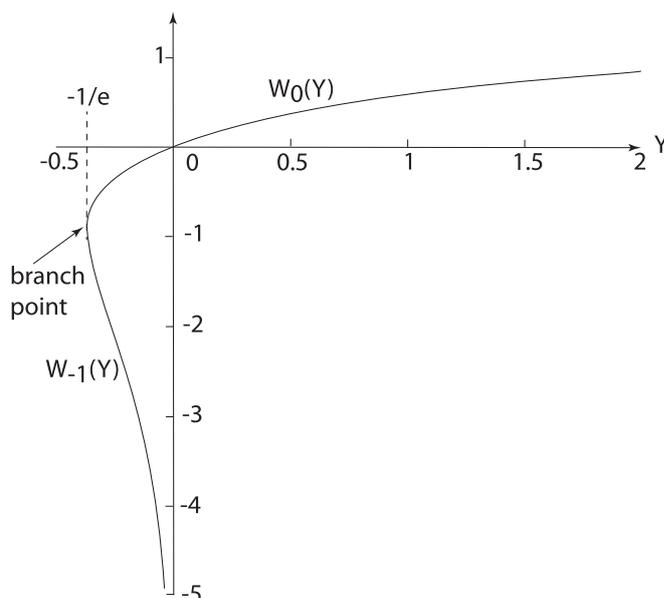
Figure 2. The real branches $W_{0,-1}(Y)$ of the Lambert W function.

$\rho(x) = -W_0(-2\widehat{Y}_l(x))/2$. Here $\widehat{Y}_l(x) = Ae^{-Kx/\varepsilon}$, with the constant A determined by matching the solutions in the boundary layer.

The main conclusion of the above analysis is that when the delivery of vesicles to synaptic targets is irreversible, with motor-cargo complexes injected at the left-hand side, there is an exponential-like decrease in the distribution of synaptic vesicles along the axon as previously observed in a model without exclusion [3], except that the decay is faster with exclusion. This indicates that exclusion effects exacerbate the preferential delivery of cargo to proximal synapses, see figure 3. A heuristic explanation is that particles move more slowly as they are blocked by exclusion, and will thus be closer to the entrance when they deliver their vesicle.

4. Reversible vesicular transport with exclusion

We now turn to our full model that combines reversible cargo delivery, exclusion effects and different motile states. As with the simpler advection–diffusion model given by equations (2.5a), we now have to keep track of motors with and without vesicular cargo. As with the previous exclusion model (section 3), we assume that each particle can only carry a single cluster of vesicles, and that exchange of vesicles is 'all-or-none.' We also assume that each particle can switch between two states, a motile state $(+)$ and a stationary state (0). When in the stationary state, the particle can reversibly exchange a vesicle with a synaptic target. Again we represent the 1D track as a lattice of N sites, labeled $i = 1, \ldots, N$, with lattice spacing $\varepsilon = L/N$, where L is the length of the track. Each site is either vacant or occupied by a particle in the motile or stationary state and with or without a vesicle. A motile particle can hop to the right if and only if the adjacent site is vacant (free of any particles). In order to keep track of whether or not a vesicle is bound to a particle, we specify the state of the site i in terms of the occupation numbers $n_i^{+,0} \in \{0, 1\}$ and $m_i^{+,0} \in \{0, 1\}$. Here $n_i^{+,0} = 1$ if the ith
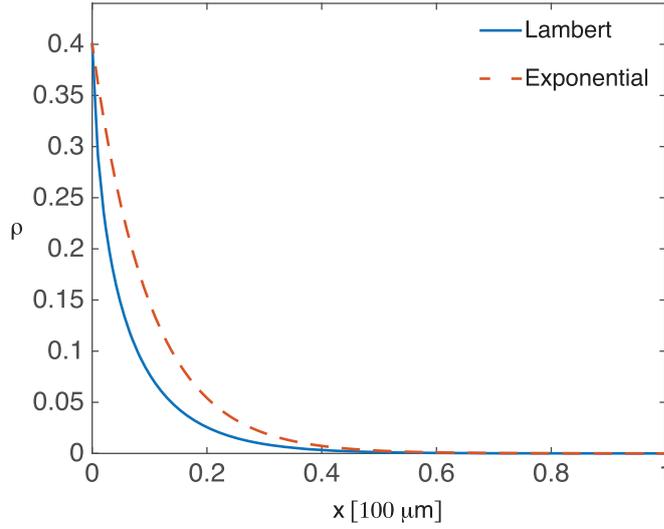
Figure 3. Comparison of the steady state solution to equation (3.8) and the decaying exponential seen in [3]. Parameter values are $\beta = 0.9$, $\varepsilon = 0.01$, and $\alpha = 0.4$.

site is occupied by a particle in state $(+, 0)$ that is carrying a vesicle, whereas $m_i^{+,0} = 1$ is the corresponding case when the particle is without a vesicle. The vacancy occupation number χ_i is then determined by the conservation law

$$\chi_i + n_i^+ + n_i^0 + m_i^+ + m_i^0 = 1.$$

The hopping rate of a particle is taken to be h if it is carrying a vesicle and by $\bar{h}$ if it is not. It remains to specify the transition rates between the different internal particle states. First, a particle can switch between the motile and stationary states with rates $\kappa_\pm$ so that

$$(n_i^+ = 1, n_i^0 = 0) \underset{\kappa_+}{\overset{\kappa_-}{\rightleftharpoons}} (n_i^+ = 0, n_i^0 = 1). \tag{4.1a}$$

and

$$(m_i^+ = 1, m_i^0 = 0) \underset{\kappa_+}{\overset{\kappa_-}{\rightleftharpoons}} (m_i^+ = 0, m_i^0 = 1). \tag{4.1b}$$
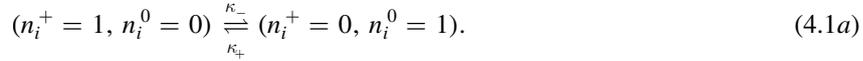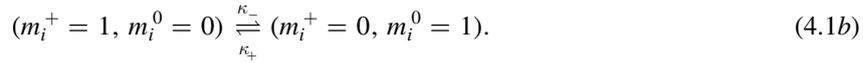
For simplicity, we take the transition rates to be the same whether or not a vesicle is bound to the particle. Second, a vesicle can be reversibly exchanged with a synaptic target according to the rates $K_\pm$ so that

$$(n_i^0 = 0, m_i^0 = 1) \underset{K_+}{\overset{K_- c_i}{\rightleftharpoons}} (n_i^0 = 1, m_i^0 = 0). \tag{4.1c}$$
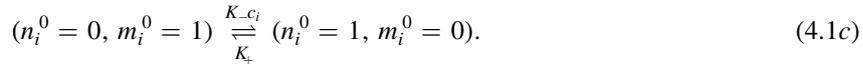
We assume that the number of vesicles c_i at the ith synaptic target is sufficiently large so that it is never depleted. Finally, particles with (without) a bound vesicle are injected on the left-hand boundary at a rate α_n (α_m), and exit the right-hand boundary at a rate β. The various processes are illustrated in figure 4.

Following along analogous lines to section 2, we represent the average with respect to all histories of the stochastic dynamics by angular brackets, and denote the density of particles with (without) a bound vesicle and in the motile state $(+)$ or stationary state (0) by $\langle n_i^{+,0}(a) \rangle$ ($\langle m_i^{+,0}(a) \rangle$). Away from the boundaries, the dynamics is described by the following system
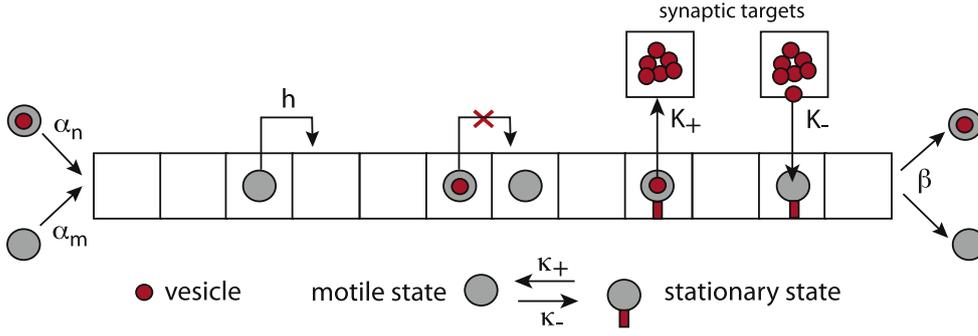
Figure 4. Dynamical rules for reversible vesicular transport: hopping, switching between motile and stationary particle states, reversible exchange of vesicles with synaptic targets, and entry/exit rates.

of equations:

$$\frac{d\langle n_i^+\rangle}{dt} = h\langle n_{i-1}^+(1 - n_i^+ - n_i^0 - m_i^+ - m_i^0)\rangle$$
$$- h\langle n_i^+(1 - n_{i+1}^+ - n_{i+1}^0 - m_{i+1}^+ - m_{i+1}^0)\rangle + \kappa_+\langle n_i^0\rangle - \kappa_-\langle n_i^+\rangle, \qquad (4.2a)$$

$$\frac{d\langle n_i^0\rangle}{dt} = -\kappa_+\langle n_i^0\rangle + \kappa_-\langle n_i^+\rangle + K_+ c_i\langle m_i^0\rangle - K_-\langle n_i^0\rangle \qquad (4.2b)$$

and

$$\frac{d\langle m_i^+\rangle}{dt} = \bar{h}\langle m_{i-1}^+(1 - n_i^+ - n_i^0 - m_i^+ - m_i^0)\rangle$$
$$- \bar{h}\langle m_i^+(1 - n_{i+1}^+ - n_{i+1}^0 - m_{i+1}^+ - m_{i+1}^0)\rangle + \kappa_+\langle m_i^0\rangle - \kappa_-\langle m_i^+\rangle, \qquad (4.2c)$$

$$\frac{d\langle m_i^0\rangle}{dt} = -\kappa_+\langle m_i^0\rangle + \kappa_-\langle m_i^+\rangle - K_+ c_i\langle m_i^0\rangle + K_-\langle n_i^0\rangle. \qquad (4.2d)$$

At the boundaries equations (4.2a) and (4.2c) become

$$\frac{d\langle n_1^+\rangle}{dt} = -h\langle n_1^+(1 - n_2^+ - n_2^0 - m_2^+ - m_2^0)\rangle + \alpha_n\langle 1 - n_1^+ - n_1^0 - m_1^+ - m_1^0\rangle,$$
$$(4.3a)$$

$$\frac{d\langle n_N^+\rangle}{dt} = h\langle n_{N-1}^+(1 - n_N^+ - n_N^0 - m_N^+ - m_N^0)\rangle - \beta\langle n_N^+\rangle, \qquad (4.3b)$$

$$\frac{d\langle m_1^+\rangle}{dt} = -\bar{h}\langle m_1^+(1 - n_2^+ - n_2^0 - m_2^+ - m_2^0)\rangle + \alpha_m\langle 1 - n_1^+ - n_1^0 - m_1^+ - m_1^0\rangle,$$
$$(4.3c)$$

$$\frac{d\langle m_N^+\rangle}{dt} = \bar{h}\langle m_{N-1}^+(1 - n_N^+ - n_N^0 - m_N^+ - m_N^0)\rangle - \beta\langle m_N^+\rangle. \qquad (4.3d)$$

Finally, given these densities, the number of vesicles at the ith synaptic target is taken to evolve according to the simple first-order kinetic scheme

$$\frac{dc_i}{dt} = K_-\langle n_i^0 \rangle - K_+ c_i \langle m_i^0 \rangle. \tag{4.4}$$

4.1. Mean-field and continuum limit

Equations (4.2a)–(4.3d) constitute a nontrivial many-body problem, since in order to calculate the time evolution of $\langle n_i^+ \rangle$ it is necessary to know the two-point correlations $\langle n_{i-1}^+ \psi_i \rangle$, where $\psi_i \in \{n_i^{+,0}, m_i^{+,0}\}$ and similarly for $\langle m_i^+ \rangle$. The latter obey dynamical equations involving three-point and four-point correlations. Thus, there is an infinite hierarchy of equations of motion. However, progress can be made by using a mean-field approximation and a continuum limit in order to derive a PDE for the densities [12, 25]. The mean-field approximation consists of replacing two-point correlations by products of single-site averages:

$$\langle n_i^+ \psi_j \rangle = \langle n_i^+ \rangle \langle \psi_j \rangle, \quad \langle m_i^+ \psi_j \rangle = \langle m_i^+ \rangle \langle \psi_j \rangle.$$

Next we set $x = k\varepsilon$, $\rho_{+,0}(x, t) = \langle n_k^{+,0}(t) \rangle$ and $\sigma_{+,0}(x, t) = \langle m_k^{+,0}(t) \rangle$. The continuum limit is then defined according to $N \to \infty$ and $\varepsilon \to 0$ such that the length of the track $L = N\varepsilon$ is fixed. (We fix length scales by setting $L = 1$). Taylor expanding $\rho_{+,0}(x \pm \varepsilon, t)$ and $\sigma_{+,0}(x \pm \varepsilon, t)$ in powers of ε,

$$\rho_0(x \pm \varepsilon, t) = \rho_0(x) \pm \varepsilon \partial_x \rho_0(x, t) + \frac{1}{2}\varepsilon^2 \partial_{xx} \rho_0(x, t) + O(\varepsilon^3)$$

etc, then gives to leading order in ε the following system of PDEs:

$$\frac{\partial \rho_+}{\partial t} = -\varepsilon \frac{\partial J_{\rho_+}(x, t)}{\partial x} + \kappa_+ \rho_0 - \kappa_- \rho_+, \tag{4.5a}$$

$$\frac{\partial \rho_0}{\partial t} = -\kappa_+ \rho_0 + \kappa_- \rho_+ + K_+ c \sigma_0 - K_- \rho_0 \tag{4.5b}$$

and

$$\frac{\partial \sigma_+}{\partial t} = -\varepsilon \frac{\partial J_{\sigma_+}(x, t)}{\partial x} + \kappa_+ \sigma_0 - \kappa_- \sigma_+, \tag{4.5c}$$

$$\frac{\partial \sigma_0}{\partial t} = -\kappa_+ \sigma_0 + \kappa_- \sigma_+ - K_+ c \sigma_0 + K_- \rho_0. \tag{4.5d}$$

The currents are

$$J_{\rho_+} = h\mathbb{L}\rho_+, \quad J_{\sigma_+} = \bar{h}\mathbb{L}\sigma_+, \tag{4.6}$$

where for any function F,

$$\mathbb{L}F = (1 - \rho - \sigma)F - \frac{\varepsilon}{2}[(1 - \rho - \sigma)\partial_x F - F\partial_x(1 - \rho - \sigma)]. \tag{4.7}$$

for $\rho = \rho_0 + \rho_+$ and $\sigma = \sigma_0 + \sigma_+$. From equations (4.3$a$)–(4.3$d$) we have the corresponding boundary conditions

$$J_{\rho_+}(0, t) = \alpha_n(1 - \rho(0, t) - \sigma(0, t)), \quad J_{\sigma_+}(0, t) = \alpha_m(1 - \rho(0, t) - \sigma(0, t)), \tag{4.8a}$$

and

$$J_{\rho_+}(1, t) = \beta\rho_+(1, t), \quad J_{\sigma_+}(1, t) = \beta\sigma_+(1, t). \tag{4.8b}$$

Finally, the continuum limit of equation (4.4) is

$$\frac{\partial c(x, t)}{\partial t} = K_- \rho_0(x, t) - K_+ c(x, t) \sigma_0(x, t). \tag{4.9}$$

4.2. Fast switching limit

We now make the additional simplification that the rates $\kappa_\pm$ of switching between the stationary and motile states are much faster than the hopping rate and $K_\pm$. This is made explicit by performing the rescalings $\kappa_\pm \to \kappa_\pm/\delta$, where δ is a second small parameter. We can then carry out a quasi-steady-state reduction of equations (4.5a) and (4.5b) by setting

$$\rho_+(x, t) = \frac{\kappa_+}{\kappa} \rho(x, t) + \delta w_+(x, t), \quad \rho_0(x, t) = \frac{\kappa_-}{\kappa} \rho(x, t) + \delta w_0(x, t),$$

and

$$\sigma_+(x, t) = \frac{\kappa_+}{\kappa} \sigma(x, t) + \delta \overline{w}_+(x, t), \quad \sigma_0(x, t) = \frac{\kappa_-}{\kappa} \sigma(x, t) + \delta \overline{w}_0(x, t),$$

with $\kappa = \kappa_+ + \kappa_-$, $w_0 + w_+ = 0$, and $\overline{w}_0 + \overline{w}_+ = 0$. Substituting these expansions into equations (4.5a)–(4.5d) gives

$$\frac{\kappa_+}{\kappa} \frac{\partial \rho}{\partial t} + \delta \frac{\partial w_+}{\partial t} = -\varepsilon \frac{\kappa_+}{\kappa} \frac{\partial J_\rho(x, t)}{\partial x} - \varepsilon \delta \frac{\partial J_{w_+}(x, t)}{\partial x} + \kappa_+ w_0 - \kappa_- w_+, \tag{4.10a}$$

$$\frac{\kappa_-}{\kappa} \frac{\partial \rho}{\partial t} + \delta \frac{\partial w_0}{\partial t} = - \kappa_+ w_0 + \kappa_- w_+$$
$$+ \frac{\kappa_-}{\kappa}(K_+ c\sigma - K_- \rho) + \delta(K_+ c\overline{w}_0 - K_- w_0), \tag{4.10b}$$

and

$$\frac{\kappa_+}{\kappa} \frac{\partial \sigma}{\partial t} + \delta \frac{\partial \overline{w}_+}{\partial t} = -\varepsilon \frac{\kappa_+}{\kappa} \frac{\partial J_\sigma(x, t)}{\partial x} - \varepsilon \delta \frac{\partial J_{\overline{w}_+}(x, t)}{\partial x} + \kappa_+ \overline{w}_0 - \kappa_- \overline{w}_+, \tag{4.10c}$$

$$\frac{\kappa_-}{\kappa} \frac{\partial \sigma}{\partial t} + \delta \frac{\partial \overline{w}_0}{\partial t} = - \kappa_+ \overline{w}_0 + \kappa_- \overline{w}_+$$
$$- \frac{\kappa_-}{\kappa}(K_+ c\sigma - K_- \rho) - \delta(K_+ c\overline{w}_0 - K_- w_0). \tag{4.10d}$$

Here $J_\rho = h\mathbb{L}\rho$, $J_\sigma = \overline{h}\mathbb{L}\sigma$ etc. Adding equations (4.10a) and (4.10b) yields

$$\frac{\partial \rho}{\partial t} = -\varepsilon \frac{\kappa_+}{\kappa} \frac{\partial J_\rho(x, t)}{\partial x} - \varepsilon\delta \frac{\partial J_{w_+}(x, t)}{\partial x} + \frac{\kappa_-}{\kappa}(K_+ c\sigma - K_- \rho) + \delta(K_+ c\overline{w}_0 - K_- w_0), \tag{4.11}$$

whereas adding equations (4.10c) and (4.10d) gives, on dropping $O(\varepsilon\delta)$ terms,

$$\frac{\partial \sigma}{\partial t} = -\varepsilon \frac{\kappa_+}{\kappa} \frac{\partial J_\sigma(x, t)}{\partial x} - \varepsilon\delta \frac{\partial J_{\overline{w}_+}(x, t)}{\partial x} - \frac{\kappa_-}{\kappa}(K_+ c\sigma - K_- \rho) - \delta(K_+ c\overline{w}_0 - K_- w_0). \tag{4.12}$$

Next we substitute for $\partial\rho/\partial t$ in equation (4.10a) using equation (4.11), substitute for $\partial\sigma/\partial t$ in equation (4.10c) using equation (4.12), and introduce the double asymptotic expansions

$$w_0 = w_{0,0} + \sum_{i,j,i+j>0} \delta^i \varepsilon^j w_{0,ij}, \quad \overline{w}_0 = \overline{w}_{0,0} + \sum_{i,j,i+j>0} \delta^i \varepsilon^j \overline{w}_{0,ij} \tag{4.13}$$

with $w_+ = -w_0$, $\overline{w}_+ = -\overline{w}_0$. The lowest order coefficients are

$$w_{0,0} = \frac{\kappa_-}{\kappa^2} \frac{\kappa_+}{\kappa} (K_+ c\sigma - K_- \rho),$$

and

$$\overline{w}_{0,0} = -\frac{\kappa_-}{\kappa^2} \frac{\kappa_+}{\kappa} (K_+ c\sigma - K_- \rho).$$

Hence, equations (4.11) and (4.12) have the leading order form

$$\frac{\partial \rho}{\partial t} = -\varepsilon \frac{\kappa_+}{\kappa} \frac{\partial J_\rho(x,t)}{\partial x} + \widehat{K}_+ c\sigma - \widehat{K}_- \rho \tag{4.14}$$

and

$$\frac{\partial \sigma}{\partial t} = -\varepsilon \frac{\kappa_+}{\kappa} \frac{\partial J_\sigma(x,t)}{\partial x} - \widehat{K}_+ c\sigma + \widehat{K}_- \rho \tag{4.15}$$

with

$$\widehat{K}_- = \frac{\kappa_-}{\kappa} K_- \left[1 + \delta(K_- + cK_+) \frac{\kappa_- \kappa_+}{\kappa^2} \right], \tag{4.16a}$$

$$\widehat{K}_+ = \frac{\kappa_-}{\kappa} K_+ \left[1 + \delta(K_- + cK_+) \frac{\kappa_- \kappa_+}{\kappa^2} \right]. \tag{4.16b}$$

Finally, equation (4.9) becomes

$$\frac{\partial c(x,t)}{\partial t} = \widehat{K}_- \rho(x,t) - \widehat{K}_+ c(x,t) \sigma(x,t). \tag{4.17}$$

We note that if $h = \overline{h}$, then adding equations (4.14) and (4.15) yields a hydrodynamic equation for the total density of particles $\phi(x,t) = \rho(x,t) + \sigma(x,t)$ identical in form to the TASEP (after rescaling):

$$\frac{\partial \phi(x,\tau)}{\partial \tau} = -\varepsilon \frac{\partial J(x,\tau)}{\partial x}, \tag{4.18}$$

with

$$J(x,\tau) = J_\rho(x,\tau) + J_\sigma(x,\tau) = \phi(x,\tau)(1 - \phi(x,\tau)) - \frac{\varepsilon}{2} \frac{\partial \phi(x,\tau)}{\partial x}, \tag{4.19}$$

and boundary conditions

$$J(0,t) = \alpha(1 - \phi(0,t)), \quad J(1,t) = \beta\phi(1,t)$$

The rescalings are

$$\tau = \varepsilon \frac{\kappa_+}{\kappa} t, \quad \alpha = \frac{\kappa}{\kappa_+}(\alpha_m + \alpha_n), \quad h = \overline{h} = 1.$$

4.3. Steady-state analysis

We now establish that a uniform, steady-state distribution of synaptic vesicles occurs when $h = \overline{h} = 1$. The steady-state equations are

$$c(x) = \frac{\widehat{K}_- \rho(x)}{\widehat{K}_+ \sigma(x)}, \tag{4.20a}$$

$$(1 - \phi)\rho - \frac{\varepsilon}{2}[(1 - \phi)\partial_x \rho + \rho \partial_x \phi] = \mathcal{J}_\rho, \tag{4.20b}$$

and

$$(1 - \phi)\sigma - \frac{\varepsilon}{2}[(1 - \phi)\partial_x \sigma + \sigma \partial_x \phi] = \mathcal{J}_\sigma. \tag{4.20c}$$

Here $\mathcal{J}_\rho$ and $\mathcal{J}_\sigma$ are constant nonequilibrium currents for the ρ and σ particles. Adding equations (4.3b) and (4.3c) yields the steady-state version of the TASEP equation (4.18):

$$\phi(1 - \phi) - \frac{\varepsilon}{2}\frac{\mathrm{d}\phi}{\mathrm{d}x} = \mathcal{J}, \tag{4.21}$$

with $\mathcal{J} = \mathcal{J}_\rho + \mathcal{J}_\sigma$. From the boundary conditions (4.8a) and (4.8b), it follows that

$$\mathcal{J}_\rho = \frac{\kappa \alpha_n}{\kappa_+ \alpha}\mathcal{J}, \quad \mathcal{J}_\sigma = \frac{\kappa \alpha_m}{\kappa_+ \alpha}\mathcal{J},$$

and, hence, equations (4.3b) and (4.3c) have the solution

$$\rho(x) = \frac{\kappa \alpha_n}{\kappa_+ \alpha}\phi(x), \quad \sigma(x) = \frac{\kappa \alpha_m}{\kappa_+ \alpha}\phi(x). \tag{4.22}$$

Finally, substituting this solution into equation (4.3a), yields the constant vesicular distribution

$$c(x) = c_0 = \frac{\widehat{K}_- \alpha_n}{\widehat{K}_+ \alpha_m}. \tag{4.23}$$

Since both densities $\sigma(x)$ and $\rho(x)$ are proportional to the steady-state solution of the standard TASEP, it is worthwhile briefly recapping the well-known properties of the latter [1, 17]. This will be useful when comparing the corresponding profiles when $h \neq \bar{h}$. Setting $q = \phi - 1/2$, the steady-state current equation (4.21) takes the form (after absorbing the factor of 2 into ε)

$$\varepsilon\frac{\mathrm{d}q}{\mathrm{d}x} = v^2 - q^2, \quad v^2 = \frac{1}{4} - J_0.$$

It follows that for $v^2 > 0$

$$\varepsilon \int \frac{\mathrm{d}q}{(v - q)(v + q)} = x - x_0,$$

where x_0 is an integration constant. Using partial fractions, we find that

$$\frac{v + q}{v - q} = \mathrm{e}^{2v(x - x_0)/\varepsilon},$$

which on rearranging yields the density profile

$$\phi(x) = \frac{1}{2} + v \tanh(v(x - x_0)/\varepsilon), \tag{4.24}$$
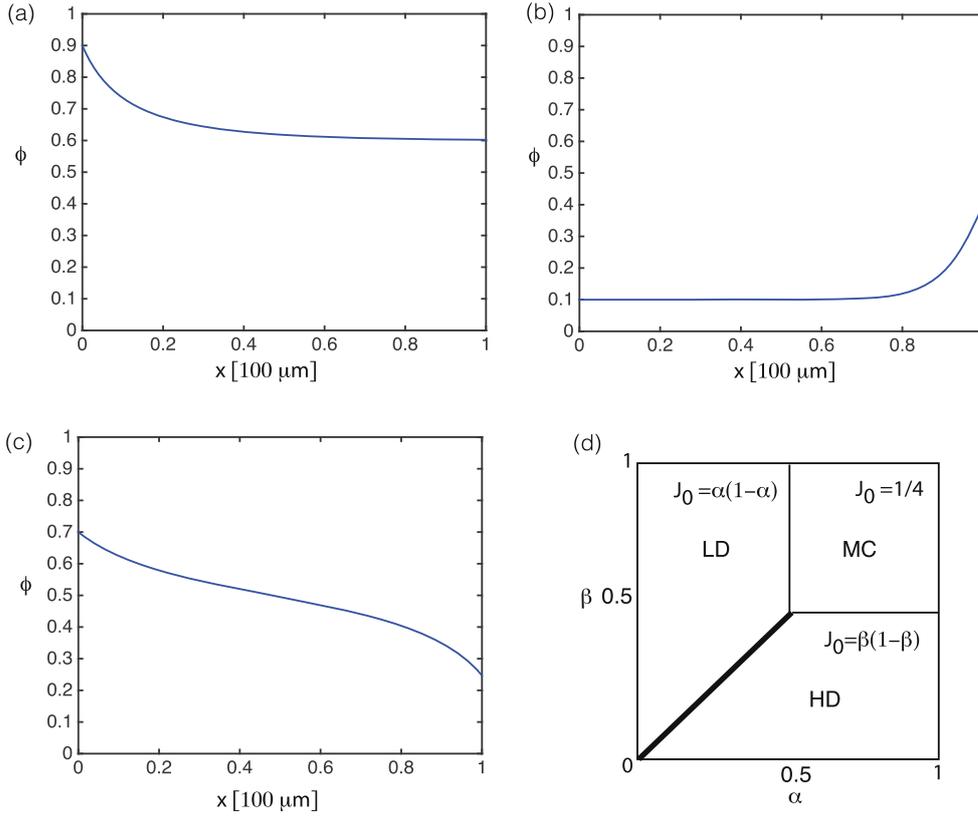
Figure 5. Steady state solutions of total density ϕ in the different phases with $\varepsilon = 0.01$ and $L = 1$. (a) Plot of ϕ in the HD phase for $\alpha = 0.9$ and $\beta = 0.3$. (b) Plot of ϕ in the LD phase for $\alpha = 0.1$ and $\beta = 0.6$. (c) Plot of ϕ in the MC phase for $\alpha = \beta = 0.7$. (d) Mean-field phase diagram for the TASEP showing the regions of α, β parameter space where the low-density (LD), high-density (HD) and maximal-current (MC) phases exist.

with $v \geqslant 0$. On the other hand, if $v^2 < 0$ then we have

$$\varepsilon \int \frac{dq}{|v^2| + q^2} = x - x_0.$$

Under the change of variables $q = \cotan(u)$, we can evaluate the integral and find that

$$\phi(x) = 0.5 + |v|\cotan(|v|(x - x_0)/\varepsilon). \tag{4.25}$$

The two unknown parameters J_0, x_0 can be determined in terms of α, β by imposing the boundary conditions at $x = 0, L$. As is well known, three distinct phases can be identified [1, 17] (see figure 5(d)):

(i) A *low density* phase in which the bulk density is smaller than $1/2$, $x_0 \approx 1$ and $v^2 > 0$. Since $\varepsilon \ll 1$, we see from equation (4.24) that $\phi(x) \approx 0.5 - v$ for all $x < x_0$. In particular, at the left-hand boundary $\alpha(0.5 + v) = J_0$, which can be rewritten as $v = J_0/\alpha - 0.5$. Squaring both sides and using the definition of v gives, to lowest order in ε,

$$\phi(0) = \alpha, \quad J_0 = \alpha(1 - \alpha), \quad \alpha < 1/2.$$

The other boundary condition becomes

$$\beta = \frac{J_0}{0.5 + v \tanh(v(L - x_0)/\varepsilon)} > \frac{J_0}{0.5 + v} = \alpha.$$

In order to satisfy this boundary condition, there is an ε-wide boundary layer at $x = L$ with $L - x_0 = O(\varepsilon)$.

(ii) A *high density* phase in which the bulk density is larger than $1/2$ and $x_0 \approx 0$. Hence, $\phi(x) \approx 0.5 + v$ in the bulk of the domain and at the right-hand boundary we have $\beta(0.5 + v) = J_0$. Following along similar lines to the low density case, we deduce that

$$\phi(L) = 1 - \beta, \quad J_0 = \beta(1 - \beta), \quad \beta < 1/2,$$

and $\beta < \alpha$. There is now a boundary layer around $x = 0$ in order to match the rate α. The two phases coexist along the line $\alpha = \beta < 1/2$.

(iii) A *maximal current phase.* In the region $\alpha > 1/2$, $\beta > 1/2$, we require $J_0 > 1/4$ so that $v^2 < 0$. It turns out that the current takes the form $J_0 = 0.25 + O(\varepsilon^2/L^2)$, that is, it is very close to the maximal value of function $\phi(1 - \phi)$. This follows from the observation that the solution (4.25) will blow up unless $0 < |v|(x - x_0)/\varepsilon < \pi$ for all $x \in [0, L]$. This implies that $x_0 = -O(\varepsilon)$ and $|v| < \pi\varepsilon/L$. Under these conditions, equation (4.25) ensures that $\phi(x) \approx 0.5$ in the bulk of the domain. The precise values of v and x_0 are then adjusted so that the boundary conditions at $x = 0, L$ are satisfied: $\phi(0) = 1 - 1/(4\alpha) > 0.5$ and $\phi(L) = 1/(4\beta) < 0.5$. Also note away from the left-hand boundary, we have $\cotan(|v|(x - x_0)/\varepsilon) \approx \varepsilon/(|v|x)$ so that

$$\phi(x) \sim 0.5 + \varepsilon/x.$$

In deriving equations (4.14) and (4.15), we first adopted the mean-field approximation used to study TASEP models with single internal states [12, 25], and then carried out an adiabatic approximation in the fast switching limit. If these approximations are valid, then we expect numerical simulations of the full stochastic model to generate a total motor density profile ϕ that converges to the classical TASEP density in the limit $\kappa_\pm \to \infty$ for $h = \bar{h}$. This is indeed found to be the case as illustrated in figure 6(c). We can see that the profile of ϕ for fast switching in the maximal current parameter regime resembles the profile for the classic TASEP model. However, as the switching slows down, the profile deviates from the TASEP curve. Nevertheless, this does not have a significant effect on the distribution of synaptic vesicles, since c is still approximately uniform, see figure 6. Interestingly, it has been shown in [33, 34] that standard mean field theory can break down for a model in which particles switch between motile and stationary states, due to statistical correlations between motile and stationary occupation numbers. Numerically , we find that this does not present a problem for our particular model when the system operates in a regime where the switching rates $\kappa_\pm$ between the motile and immotile states of the motors are fast compared to the hopping rate h and rates of exchange of vesicles between motors and synapses $K_\pm$.

Note that figure 6 and subsequent numerically generated figures are obtained using a continuous-time Monte Carlo algorithm based on the Gillespie algorithm [6, 35] and the dynamical rules elucidated in figure 4. Individual particles carrying cargo that are bound to a microtubule can move to the adjacent site at a rate h provided the adjacent site is unoccupied. Particles not carrying cargo but bound to a microtubule can move to the adjacent site provided it is empty at a rate $\bar{h}$. Individual particles may bind and unbind from a microtubule at the
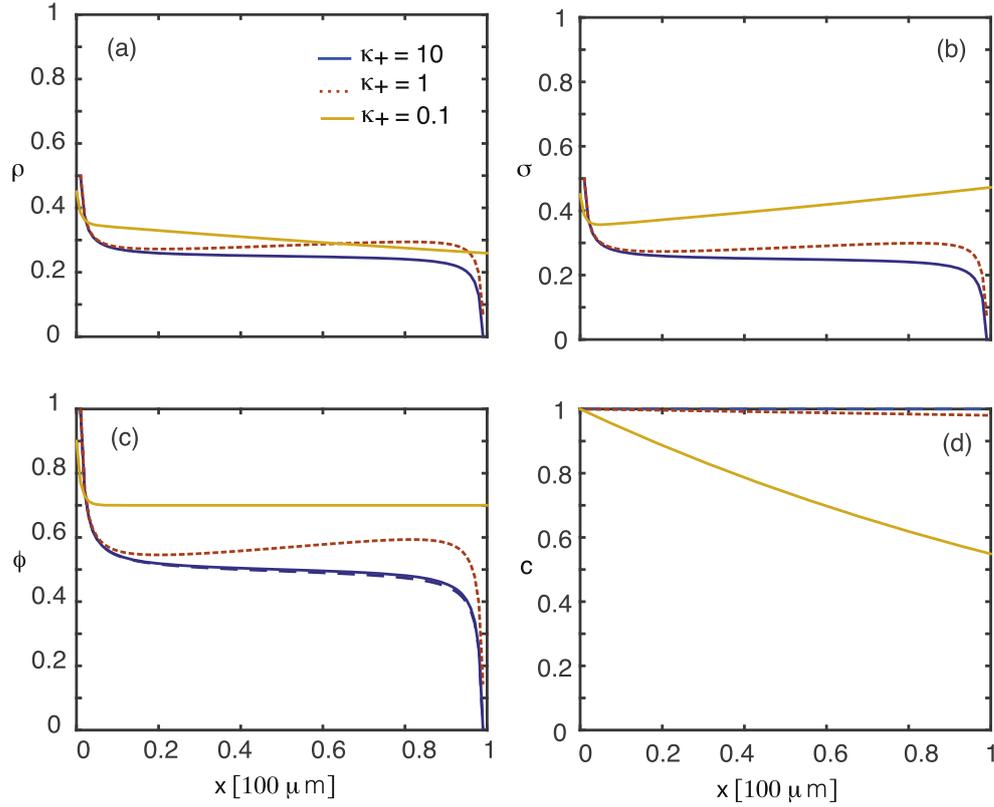
Figure 6. Effect of slowing down the switching rates between motile and immotile states on concentration profiles when TASEP limit is in a maximum current phase (dashed curve of (c)). Plots of (a) ρ, (b) σ (c) total motor density ϕ, and (d) and synaptic vesicle density c for various switching rates $\kappa_- = \kappa_+$. Other parameter values are $\alpha_n = \alpha_m = 0.8$, $\beta = 0.8$, $K_\pm = 0.5$, $h = \bar{h} = 1$, and $N = 100$.

rates $\kappa_\pm$ and particles unbound from microtubules may deliver vesicles at a rate K_- or recover them at a rate K_+. We collect statistics from the system once it has reached steady state. To ensure it has reached steady state, we neglect the first 10^8 steps and collect statistics on the subsequent 10^8 steps.

4.4. Disparity in hopping rates

In the case where $h \neq \bar{h}$, adding together equations (4.14) and (4.15) yields

$$\frac{\partial \phi}{\partial t} = -\varepsilon \left[\frac{\partial J_\rho}{\partial x} + \frac{\partial J_\sigma}{\partial x} \right],$$

which cannot be easily analyzed. Nevertheless, the time evolution of the system can be understood by performing Monte Carlo simulations of the full stochastic model as summarized above. We find that the value of $H \equiv \bar{h} - h$ alters the nature of the distribution of vesicles along the axon. This is illustrated in figures 7–9, which correspond respectively to the LD, HD and MC phases for ϕ in the limit $h = \bar{h} = 1$. In each figure, we plot the density profiles of ρ, σ, ϕ and c for various hopping rates $h < \bar{h} = 1$. It can be seen that in each case,
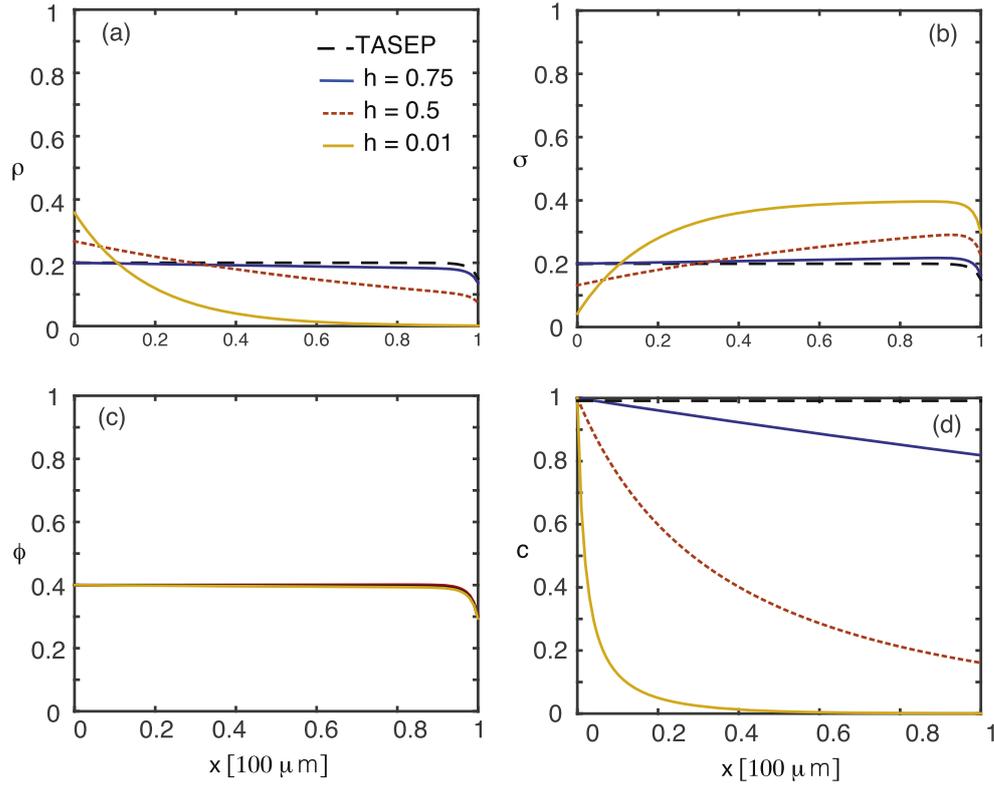
Figure 7. Effect of disparity in hopping rates on concentration profiles when TASEP limit is in a low density phase. Plots of (a) ρ, (b) σ (c) total motor density ϕ, and (d) and synaptic vesicle density c for various hopping rates $h \leqslant \overline{h} = 1$. Other parameter values are $\alpha_m = \alpha_n = 0.4$, $\beta = 0.7$, $K_\pm = 0.5$, $\kappa_\pm = 10$, and $N = 100$.

as h decreases (H increases), the distribution c of synaptic vesicles along the axon develops an exponential-like decay with respect to x. This reflects the fact that the ratio $\rho(x)/\sigma(x)$ is no-longer x-independent. When $h = \overline{h}$ the synaptic vesicle concentration is uniform, $c(x) = 1$ We conclude that achieving synaptic democracy is also dependent on the motility of the motor-cargo complexes relative to the motility of the particles without vesicles. In all the stochastic simulations we take h, the hopping rate of vesicle-bound particles, to be at most $\overline{h}$, the hopping rate of particles without vesicles, which corresponds to the intuition that the former would naturally move slower than the latter due to the added load. Hence, there is a correlation between the value of h and the specific type of cargo being delivered. If, for example, the cargo of a motor is too large, then we expect $h \ll \overline{h}$, and the distribution of the given cargo along the axon may not be uniform. On the other hand, if the cargo is relatively small, then $h \approx \overline{h}$ and synaptic democracy can be achieved. Analogous results were found in [3] for the simpler model without exclusion.

5. Relationship to other exclusion process models

Equations (4.14) and (4.15) closely resemble the hydrodynamic equations that arise in modeling processes that account for exclusion effects as well as internal states. For example,
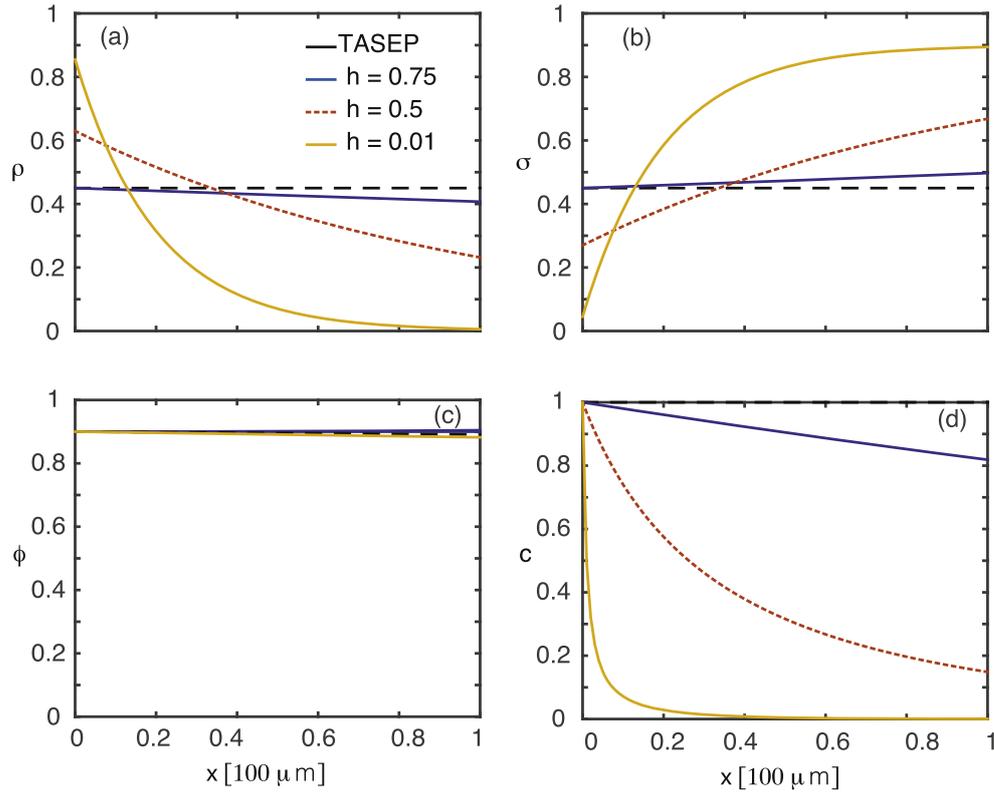
Figure 8. Effect of disparity in hopping rates on concentration profiles when TASEP limit is in a high density phase. Plots of (a) ρ, (b) σ (c) total motor density ϕ, and (d) and synaptic vesicle density c for various hopping rates $h \leqslant \overline{h} = 1$. Other parameter values are $\alpha_m = \alpha_n = 0.9$, $\beta = 0.1$, $K_{\pm} = 0.5$, $\kappa_{\pm} = 10$, and $N = 100$.

Reichenbach *et al* [27, 28] allow for particles in each lattice site to exist in one of two internal 'spin' states, see figure 10. Particles with opposite spins can occupy the same lattice point and can move to the next lattice site at a prescribed rate provided the adjacent site is not already occupied by another particle of the same spin state. Hence, each particle respects the Pauli exclusion principle. Another common interpretation for these internal states is that of a car traveling on one lane of a two-lane highway. In this context, each lattice site corresponds to a segment of the highway, and thus can be occupied by two cars so long as they are not on the same lane. In either of the interpretations, particles are allowed to switch states provided they are alone in occupying a given site. Note that the effects of exclusion on collective vesicle transport has also been analyzed by Muhuri and Pagonabarraga. They consider the case of bidirectional transport in which particles can reverse direction and reversibly bind to the filament [22]. However, the authors do not separately model vesicles and molecular motors.

In our work, we provide a new biophysical example of internal states within the context of exclusion processes. The full model without the application of the adiabatic approximation consists of particles in one of four internal states: (i) a motile particle bound to the track and carrying a vesicle, (ii) a motile particle bound to the track without a vesicle, (iii) a stationary particle unbound from the track but carrying a vesicle, and (iv) a stationary particle unbound from the track without a vesicle. One important difference between the spin and traffic models
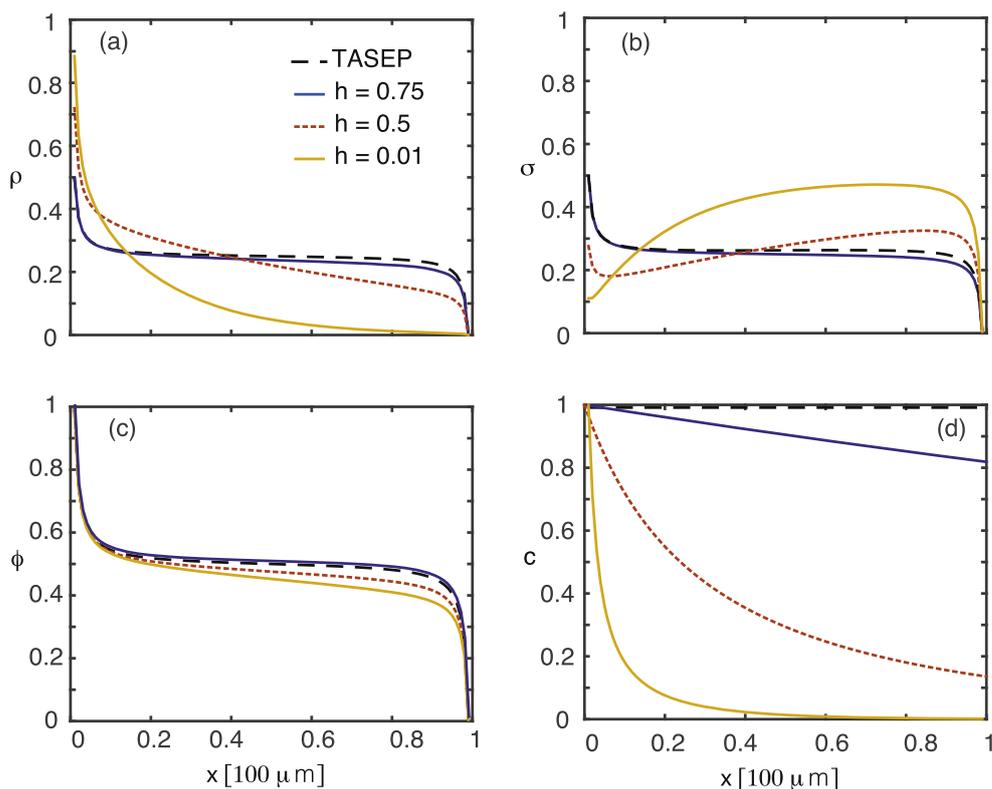
Figure 9. Effect of disparity in hopping rates on concentration profiles when TASEP limit is in a maximum current phase. Plots of (a) ρ, (b) σ (c) total motor density ϕ, and (d) and synaptic vesicle density c for various hopping rates $h \leqslant \bar{h} = 1$. Other parameter values are $\alpha_m = \alpha_n = 0.9$, $\beta = 0.7$, $K_{\pm} = 0.5$, $\kappa_{\pm} = 10$, and $N = 100$.
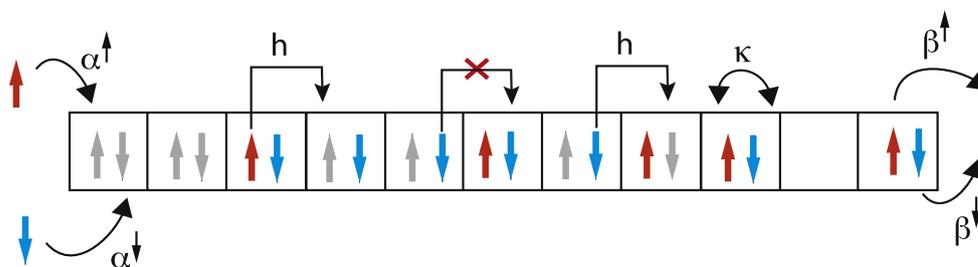
Figure 10. Dynamical rules for an exclusion model with two internal spin states [27, 28]. Particles in up (down) states enter with rates $\alpha^{\uparrow}$ ($\alpha^{\downarrow}$), move unidirectionally to the right with hopping rate h, flip spin state at a rate κ, and leave the system at rates $\beta^{\uparrow}$ ($\beta^{\downarrow}$). Pauli's exclusion principle holds at every lattice site.

and ours lies in the definitions of the currents in each model. In spite of the existence of two internal states in the two-lane traffic traffic and spin models, the currents are nevertheless the same as seen in standard TASEP models. That is, if $\rho_i(x, t)$ is the density of a particle in the ith internal state, its current is given by, for example, an expression of the form $\rho_i(1 - \rho_i)$.

This arises from the fact that double occupation of a single lattice site is allowed provided each particle exists in a different internal state. In our model, currents take a more restrictive form, since a motor can only hop to the adjacent site if it is completely unoccupied. Hence, the currents in our model have the form shown in equation (4.7). Differences in the currents persist when we use an adiabatic approximation to reduce the full model to a model with two-internal states (particles with or without a vesicle).

6. Discussion

In this paper, we investigated the biophysical machinery involved in maintaining synaptic democracy in axons. In particular, we generalized the results found in [3] by examining the effects of exclusion on the distribution of synaptic vesicles along an axon. For both the irreversible and reversible delivery cases, we modeled the dynamics of motor-cargo complexes in terms of the equations of motion for the average occupation numbers at each site on a 1D lattice. By invoking the mean field approximation, we derived a system of hydrodynamic equations which were used to determine the steady state distributions of both motor-cargo complexes and synaptic vesicles. In the irreversible case, we found that exclusion exacerbates the preferential delivery of vesicles to synaptic sites near the soma. In the reversible case, we performed an adiabatic approximation on the system of hydrodynamic equations by assuming that switching between internal states is fast compared to ballistic dynamics. We found that the steady state distribution of vesicles is now approximately uniform, provided that the speed of a particle is only weakly dependent on whether or not it is carrying a vesicle.

There are a number of issues we wish to explore in future work. One assumption we made was that each motor-cargo complex only carried one SVP, and that the underlying complex persists when the SVP is delivered. A more realistic scenario is to allow each complex to carry multiple SVPs, so that there is reversible exchange of vesicles between a persistent complex and a target [21]. Some modeling work has been done in this area using aggregation theory and a modified version of the well-known Becker–Doring equations [4], but exclusion effects were not taken into account. Another important generalization would be to investigate what happens when we allow for bidirectional motor transport. There is considerable debate in the literature regarding the most likely mechanism for bidirectional transport [29–31]: (a) an asymmetric *tug-of war model* involving the joint action of multiple kinesin and dynein motors pulling in opposite directions; (b) a symmetric tug-of-war model where all the motors are of the same type, but they are distributed on microtubules of opposite polarity; (c) a hopping model, in which the whole motor-cargo complex hops between microtubules of opposite polarity; (d) some form of coordination complex that controls the switching between different motor species. Yet another extension of our work would be to explore the effects of heterogeneity where, for example, the distribution and size of synaptic targets are not uniform. Finally, we hope to investigate the impact of exclusion effects on other biological processes that involve axonal transport. For example, we recently developed a mathematical model of a molecular motor-based axonal length sensing mechanism using delay differential equations and advection–diffusion PDEs [32], but did not incorporate exclusion effects.
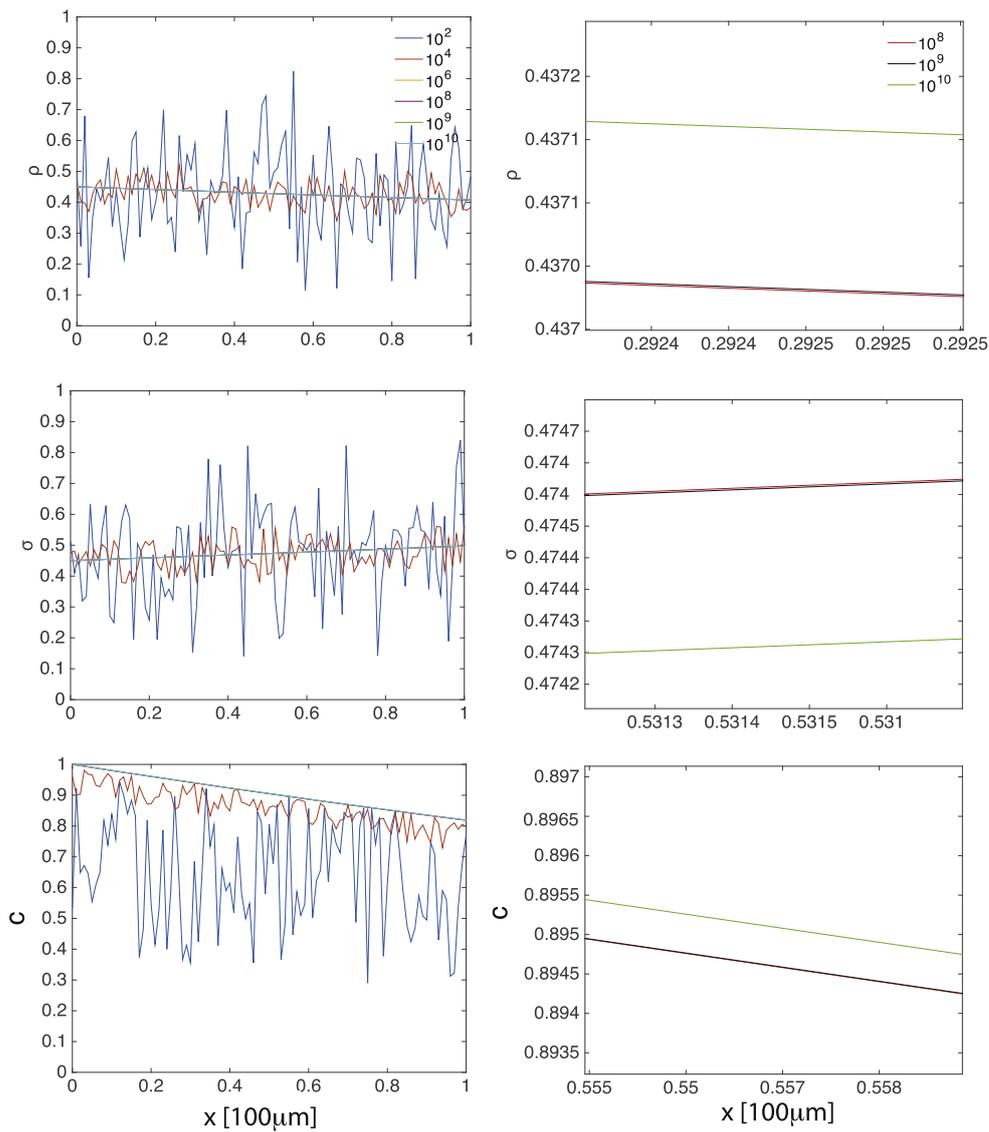
Figure 11. Left column: profiles of ρ, σ, and vesicle density $c(x, t)$ after the Gillespie algorithm has run for the specified number of time steps for $h = 0.75$. Right column: blowup of the curves at large times. Other parameter values are as in figure 8.

Appendix

In this appendix, we show some simulation results that provide evidence for the convergence of the profiles to their respective steady states. We focus on the results from figure 8. We show plots that provide snapshots of the system as it progresses through time up to 10^{10} time steps. For $h = 0.75$ all the curves appear to converge by 10^6 time steps, as running the system longer does not drastically change the profiles (see figure 11). This is further illustrated by
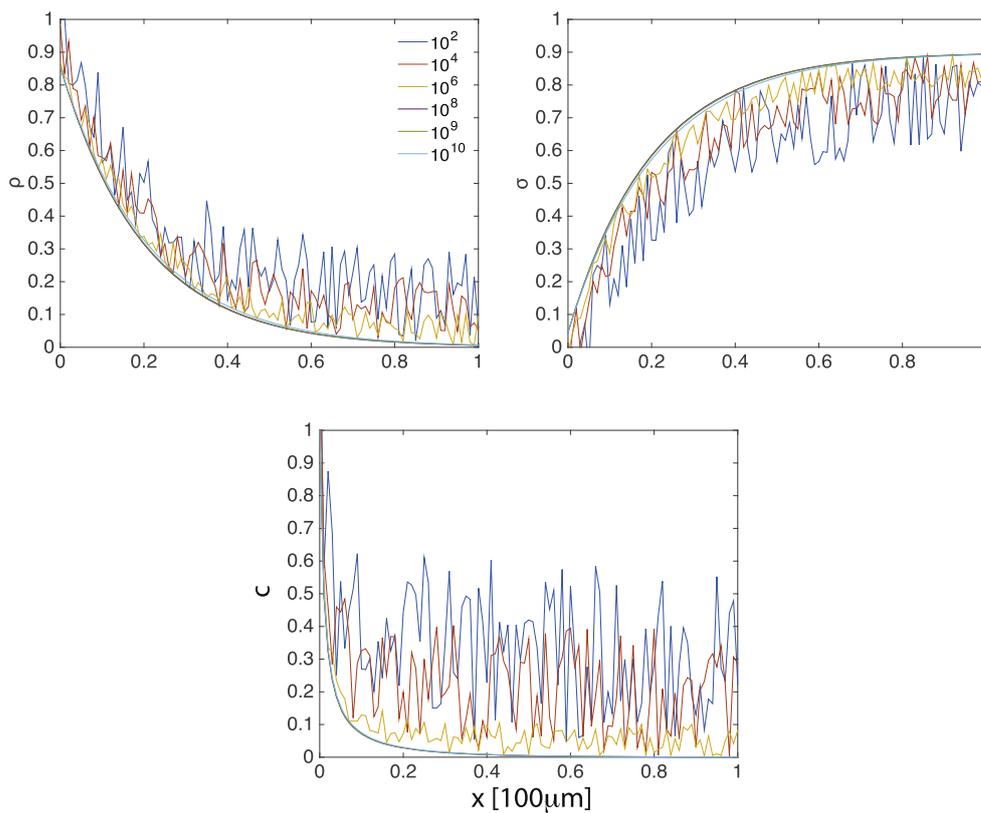
Figure 12. Profiles of ρ, σ, and vesicle density $c(x, t)$ after the Gillespie algorithm has run for the specified number of time steps for $h = 0.01$. Other parameter values are as in figure 8.

zoomed in plots. Note that the plots for $h = 0.01$ converge more slowly, but 10^8 steps appears sufficient (see figure 12).

References

[1] Blythe R A and Evans M R 2007 Nonequilibrium steady states of matrix-product form: a solver's guide *J. Phys. A: Math. Theor.* **40** R333–441
[2] Bressloff P C 2014 *Stochastic Processes in Cell Biology* (New York: Springer)
[3] Bressloff P C and Levien E 2015 Synaptic democracy and active intracellular transport in axons *Phys. Rev. Lett.* **114** 168101
[4] Bressloff P C 2016 Aggregation-fragmentation model of vesicular transport in neurons *J. Phys. A: Math. Theor.* **49** 145601
[5] Chou T, Mallick K and Zia R K P 2011 Non-equilibrium statistical mechanics: from a paradigmatic model to biological transport *Rep. Prog. Phys.* **74** 116601
[6] Ciandrini L, Romano M C and Parmeggiani A 2014 Stepping and crowding of molecular motors: statistical kinetics from an exclusion process perspective *Biophys. J.* **107** 1176
[7] Corless R, Gonnet G, Hare D, Jeffrey D and Knuth D 1996 On the Lambert *W* function *Adv. Comput. Math.* **5** 329
[8] De Vas K J, Grierson A J, Ackerly S and Miller C C 2008 Role of axonal transport in neurodegenerative diseases *Ann. Rev. Neurosci.* **31** 151–73

 [9] Derrida B, Domany E and Mukamel D 1992 An exact solution of a one-dimensional asymmetric exclusion model with open boundaries *J. Stat. Phys.* **69** 667

[10] Derrida B, Evans M R, Hakim V and Pasquier V 1993 Exact solution of a 1D asymmetric exclusion model using a matrix formulation *J. Phys. A: Math. Gen.* **26** 1493

[11] Derrida B 1998 An exactly soluble nonequilibrium system: the asymmetric simple exclusion process *Phys. Rep.* **301** 65

[12] Evans M R, Juhasz R and Santen L 2003 Shock formation in an exclusion process with creation and annihilation *Phys. Rev.* E **68** 026117

[13] Hirokawa N and Takemura R 2005 Molecular motors and mechanisms of directional transport in neurons *Nat. Rev. Neurosci.* **6** 201–14

[14] Hoerndli F J, Maxfield D A, Brockie P J, Mellem J E, Jensen E, Wang R, Madsen D M and Maricq A V 2013 Kinesin-1 regulates synaptic strength by mediating the delivery, removal, and redistribution of AMPA receptors *Neuron* **80** 1421–37

[15] Howard J 2001 *Mechanics of Motor Proteins and the Cytoskeleton* (Sunderland, MA: Sinauer Associates Inc.)

[16] Kennedy M J and Ehlers M D 2006 Organelles and trafficking machinery for postsynaptic plasticity *Ann. Rev. Neurosci.* **29** 325

[17] Krug J 1991 Boundary-induced phase transitions in driven diffusive systems *Phys. Rev. Lett.* **67** 1882–1185

[18] Lemieux M, Labrecque S, Tardif C, Labrie-Dion E, LeBel E and De Koninck P 2012 Translocation of CaMKII to dendritic microtubules supports the plasticity of local synapses *J. Cell Biol.* **198** 1055–73

[19] Hoerndli F J, Maxfield D A, Brockie P J, Mellem J E, Jensen E, Wang R, Madsen D M and Maricq A V 2013 Kinesin-1 regulates synaptic strength by mediating the delivery, removal, and redistribution of AMPA receptors *Neuron* **80** 1421–37

[20] Maeder C I, San-Miguel A, Wu E Y, Lu H and Shen K 2014 In vivo neuron-wide analysis of synaptic vesicle precursor trafficking *Traffic* **15** 273–91

[21] Maeder C I, Shen K and Hoogenraad C C 2014 Axon and dendritic trafficking *Curr. Opin. Neurobiol.* **27** 165–70

[22] Muhuri S and Pagonabarraga I 2008 Collective vesicle transport on biofilaments carried by competing molecular motors *Europhys. Lett.* **84** 58009

[23] Newby J M and Bressloff P C 2010 Quasi-steady state reduction of molecular motor-based models of directed intermittent search *Bull. Math. Biol.* **72** 1840–66

[24] Parmeggiani A, Franosch T and Frey E 2003 Phase coexistence in driven one-dimensional transport *Phys. Rev. Lett.* **90** 086601

[25] Parmeggiani A, Franosch T and Frey E 2004 Totally asymmetric simple exclusion process with Langmuir kinetics *Phys. Rev.* E **70** 046101

[26] Wong M Y, Zhou C, Shakiryanova D, Lloyd T E, Deitcher D L and Levitan E S 2012 Neuropeptide delivery to synapses by long-range vesicle circulation and sporadic capture *Cell* **148** 1029–38

[27] Reichenbach T, Franosch T and Frey E 2006 Exclusion processes with internal states *Phys. Rev. Lett.* **97** 050603

[28] Reichenbach T, Frey E and Franosch T 2007 Traffic jams induced by rare switching events in two-lane transport *New J. Phys.* **9** 159

[29] Gross S P 2004 Hither and yon: a review of bi-directional microtubule-based transpor *Phys. Biol.* **1** R1–11

[30] Kural C, Kim H, Syed S, Goshima G, Gelfand V I and Selvin P R 2005 Kinesin and dynein move a peroxisome in vivo: a tug-of-war or coordinated movement? *Science* **308** 1469–72

[31] Muller M J I, Klumpp S and Lipowsky R 2008 Tug-of-war as a cooperative mechanism for bidirectional cargo transport by molecular motors *Proc. Natl Acad. Sci. USA* **105** 4609–14

[32] Karamched B R and Bressloff P C 2015 A delayed feedback model of axonal length sensing *Biophys. J.* **108** 2408–19

[33] Pinkoviezky I and Gov N S 2013 Modelling interacting molecular motors with an internal degree of freedom *New J. Phys.* **15** 025009

[34] Pinkoviezky I and Gov N S 2013 Transport dynamics of molecular motors that switch between an active and inactive state *Phys. Rev.* E **88** 022714

[35] Gillespie D T 1977 Exact stochastic simulation of coupled chemical reactions *J. Phys. Chem.* **81** 23402361